

ZnS Nanogenerator for Biomechanical Energy Harvesting: Towards Sustainable Power Generation

Syam Sundar G¹, A Muthuvel¹, Gollangi Jogi Naidu¹, Balan S^{1*}

¹*Department of Electrical and Electronics Engineering, Indian Institute of Industry Interaction Education and Research, Chennai, Tamil Nadu 600066
Email: iiiiier.info.journals@gmail.com

Abstract:

A new TENG was constructed with low-cost inorganic materials, including the ZnS nanosheet films and PDMS as the primary triboelectric layers. The novelty of this research lies in the use of pure ZnS nanosheets and the PDMS-Al cover foils. By using manual excitation, the TENG delivered an output voltage of about 8.0 V and a short circuit current of about 7.12 μ A. The performance of the proposed device was also impressive in the sense that it was able to cycle 1000 times without a significant decline in efficiency. The versatility of the TENG is apparent, as the fabricated TENG successfully charged portable electronic devices such as a digital clock, thermometer, calculator, and a series of 64 LEDs through capacitor storage. Also, the TENG demonstrated aptitude in force and pressure sensing, where the output could act as the clock signal for digital systems. This work demonstrates that ZnS-based TENGs could be useful for effective biomechanical energy collection and sensing in the future.

Keywords — Triboelectric Nanogenerator (TENG), ZnS nanosheet films, Polydimethylsiloxane (PDMS), Output voltage (8 V), Short-circuit current (7.12 μ A) Force and pressure sensing

I. INTRODUCTION

Triboelectric nanogenerators (TENG) have been in the spotlight for the last 10 years or more because of all the ways they may be used in electronics, medicine, sensing, AI, and more [1]-[4]. It has been shown that the Triboelectric nanogenerators can transform several forms of mechanical power into electrical power, including ocean, wind, and biomechanical energies. This leads many to believe that triboelectric nanogenerators technique is a viable renewable energy option [5, 6]. It is possible to produce energy from low-frequency irregular input energies is only one of the many benefits of TENGs, which also include a simple design, cheap cost, durability, and scaling [7], [8]. Combining electrostatic induction with triboelectrification, the Triboelectric nanogenerators is a newer method of energy

collection that can convert mechanical energy into electrical [9]. When two surfaces in TENG come into periodic contact and then separate again due to external mechanical force, electrical energy is generated [10]. As discussed in Chapter 1, four different forms of triboelectric nanogenerators operation have been suggested, depending on the configuration of the electrodes and polarizing switch direction.

II. RELATED WORK

Several triboelectric materials demonstrate the vertical contact separation mode, among others [11], [12]. Hence, in order to collect energy for our Triboelectric nanogenerators activity in this chapter, the vertical contact separation process was used. The electricity provided by Triboelectric nanogenerators was used to run a number of small electrical gadgets and sensors. The downsides of

Triboelectric nanogenerators are their difficult production methods, poor surface triboelectric charge density, lower flexibility, and lower power density, as well as the fact that they entail several layers. To improve Triboelectric nanogenerators power density, some authors have suggested multiple methods, such as: (1) making the surface rougher or raising the effective contact area [13], [14], and (2) using different methods to modify the surface [15]. Using a chain reaction of several Triboelectric nanogenerators is a simple approach to increase the power of their output. Using different materials or combinations for the active layer is a typical way to increase the output power of triboelectric nanogenerators . According to a plethora of research, novel inorganic functional substances, metal oxides, sulfides, and combinations of these, have taken the cake when it comes to enhancing the effectiveness of Triboelectric nanogenerators. Inorganic functional materials that are highly electrically conductive, have a wide surface area, and exhibit great stability chemically might significantly enhance Triboelectric nanogenerators efficiency.

Polyvinylidene fluoride (PVDF) and polylactic acid (PLA) are only two of the many polymers that have been used to create Triboelectric nanogenerators. Not long ago, triboelectric nanogenerators were made from bio-waste materials such rice husks, fish scales, orange peels, and fish bladders. The construction of Triboelectric nanogenerators for use in clothing was inspired by the design and construction of textiles. In this study, we provide a novel tribo material for Triboelectric nanogenerators manufacturing based on ZnS nanosheets. Work on new triboelectric couplings is ongoing and has the potential to significantly impact energy efficiency, as well as the affordability and complexity of triboelectric nanogenerator (TENG) systems. Many research efforts in recent years have devoted their attention to investigating novel triboelectric material combinations for use in energy harvesting. In this section, we provide a novel triboelectric pair for mechanical energy harvesting, which consists of intrinsic ZnS nanosheets and PDMS film. Electrode materials included an aluminum substrate and foil

from discarded food packaging (FPAC). On the other hand, using pure ZnS and nanosheet morphology was not done by anybody, and there were only a few of papers on ZnS-based Triboelectric nanogenerators in Table 1.

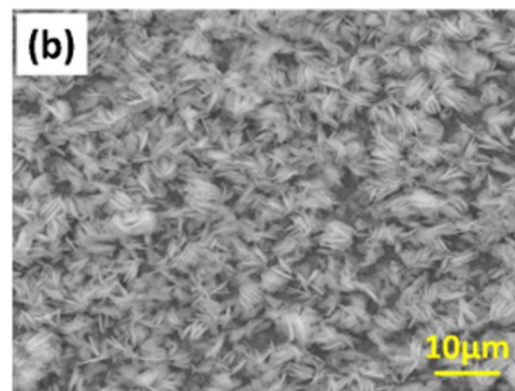
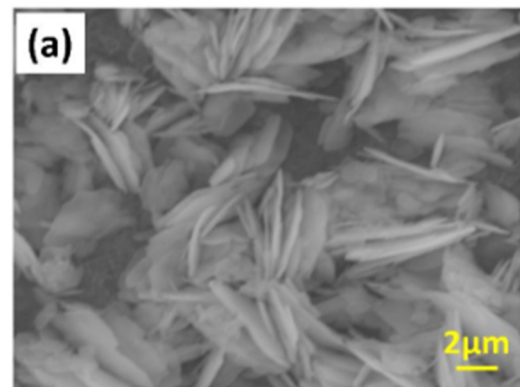
In addition, zinc sulfide (ZnS) is an intriguing semiconducting conductor that shows promise in many different fields. Some examples of these fields are photocatalysis, optoelectronic devices, micro force active sensors, and ultraviolet (UV) nanolasers. Compared to ZnO, BaTiO₃, CdSe, GaN, and PZT, ZnS has not been extensively investigated for its potential use in nanogenerators, despite its piezoelectric and triboelectric characteristics. Regarding the Triboelectric nanogenerators design aspect, the charge transfer rate between 2 tribo layers may be considerably improved by ultra-thin ZnS NSs. Possible future uses for the suggested ZnS-based Triboelectric nanogenerators include photodetector and self-powered gas systems. Also, compared to other nanostructure types, ZnS nanosheet films have superior structural stability, which is why they were chosen for Triboelectric nanogenerators. There are a number of benefits to fabricating Triboelectric nanogenerators with ZnS as described in this chapter. Firstly, there is no need for an additional electrode deposition step because ZnS nanosheets grow directly on the aluminum material. Secondly, a strong bond of ZnS nanosheets is formed because they grow directly on the aluminum material. Lastly, unlike seed layer supported ZnS nanorods and nanowires, ZnS nanosheets growth does not require an extra seed layer. The ZnS nanosheet structure was selected for additional investigations based on the reasons mentioned above.

Table 1: Performance Metrics of Various ZnS-Based Energy Harvesting Devices

Substances	Device Size (cm ²)	O/P Performance	Classification	Structure

ZnS /PD MS	3×3	27 Volts, 0.2 μA	TENG	Fabric
PDMS/ZnS	4×1.5	114.3Volts 176.6 nA	TIEL	Particle
ZnS/ZnO	3×3	156Volts, 21.9 μA/cm ²	TENG	Nanoflakes
ZnS	4×3	Unavailable	TIEL	Particle
ZnS/PD MS	4×4 cm ²	7 Volts, 6.21 μA; 23 Volts	TENG	Nanosheets

Moreover, the EDX spectrum of the obtained ZnS nanosheets shown in Figure 1(c) only revealed Zn, S, and Al elements, proving the pureness of the nanosheets. The crystalline phase of the synthesized ZnS sample was further characterized for its crystal structure using X-ray Diffraction (XRD). Figure 1(d) depicts the XRD patterns of the ZnS nanostructure film. The diffraction peak at 29.32° proves the crystalline nature of the cubic ZnS. The strong diffraction peaks at 38.59°, 44.85°, 65.24°, and 78.35° can be attributed to the (111), (020), (022), and (131) planes of cubic bare Al derived from the substrate (JCPDS No. #85-1327). The additional diffraction peak at 20° and the corresponding (006) plane confirms the formation of ZnAl₂S₄ at the interface of ZnS nanostructures and aluminum [50].

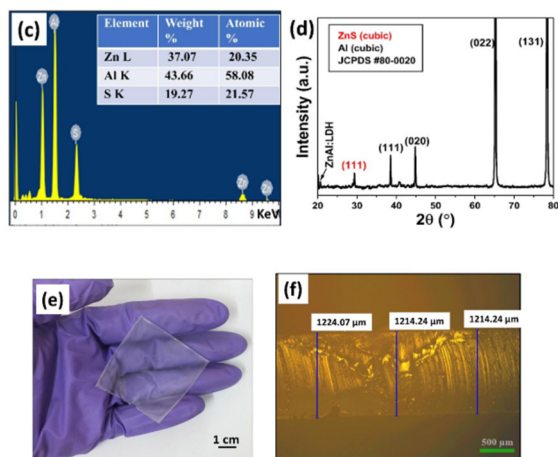


Conversely, Triboelectric Nanogenerator is often constructed using PDMS, a polymer film, as a negative triboelectric layer. The fabrication of Triboelectric Nanogenerator has also shown promise for use in digital systems, sensors, and electronics

III. PROPOSED WORK

To begin with, a TENG with a size of 3 cm x 3 cm and a gap of 1 cm was fabricated. A gap of 3 cm between the tribo layers was used with the hand-tapping frequency of 4 Hz. Moreover, the study also provided a comprehensive understanding of the effects of the active area of tribo layers, the distance between the layers, the frequency of the applied force, and the variation of the force on the output voltage of the TENG. Figure 1 a-b: The surface morphology of ZnS film deposited on aluminum substrate: at 160°C, 15, 000X and 3, 000X respectively. These images indicate the even dispersion of ZnS nanosheets on the Al substrate.

Figure 1(e) shows the photographs of synthesized transparent PDMS film. As shown in figure 1(f) the film thickness of the PDMS was measured using an optical microscope and it was found to be around 1.2 mm.



In Figure 1, we can see the following: (a-b) various resolutions of the as-synthesized ZnS film on an Al substance, (c) the EDX spectrum and XRD spectra of the ZnS nanosheet film, (e) the original pictures of the PDMS films that were made, and (f) a cross-sectional image of the PDMS with the use of an optical microscope.

Fig 2 (a) shows transmission electron microscopy (TEM) picture of ZnS nanosheets. The image suggests the nanosheet-like morphology with an average width of 0.429 ± 0 . I found the particle size distribution to be around $0.15 \mu\text{m}$; this is in accordance to the scanning electron microscopy (SEM) images. High-resolution TEM image of ZnS nanosheet showing its polycrystalline nature is shown below in Fig.2 (b). Moreover, the selected-area electron diffraction (SAED) pattern in Figure 2(c) also shows some rings of diffractions, which also approve the polycrystalline nature of ZnS nanosheets. The EDX spectrum of a single ZnS nanosheet is also shown in Figure 2(d) which exhibits Zn, S, Cu, C, and Al peaks confirming the presence of ZnS nanosheets. Cu and C are from the copper grid and air-borne carbon while Zn, S, and Al are from the ZnS nanosheets. The observed Al could be contributed by the doping of the ZnS nanosheets or Al particles which might have been incorporated during the preparation of the TEM samples.

This indicates that further work is required to determine whether the ZnS film is doped or not. The average surface roughness of ZnS and PDMS surfaces was investigated using an atomic force microscope (AFM), as demonstrated in Figure 2(e,f). From the profilometry analysis, the average surface roughness was established to be 184 nm for ZnS and 49 nm for Cr. 8 nm for PDMS. For instance, the surface roughness values of the ZnS film are found to be about four times that of the PDMS surface due to the irregularities in the nanosheet

structure. Furthermore, incorporation of ZnS nanosheets on the Al substrate improved the surface area by up to 18-%. From the above Auger spectra, it can be found that the intensity of the Auger spectrum of the Aluminum layer is slightly lower than 1% compared to a pure Al substrate. SEM analysis also supported the AFM results on the surface roughness of the denture base material. Surface roughness is vital in the output voltage of the TENG as the operation of the device hinge on triboelectrification, and electrostatic induction.

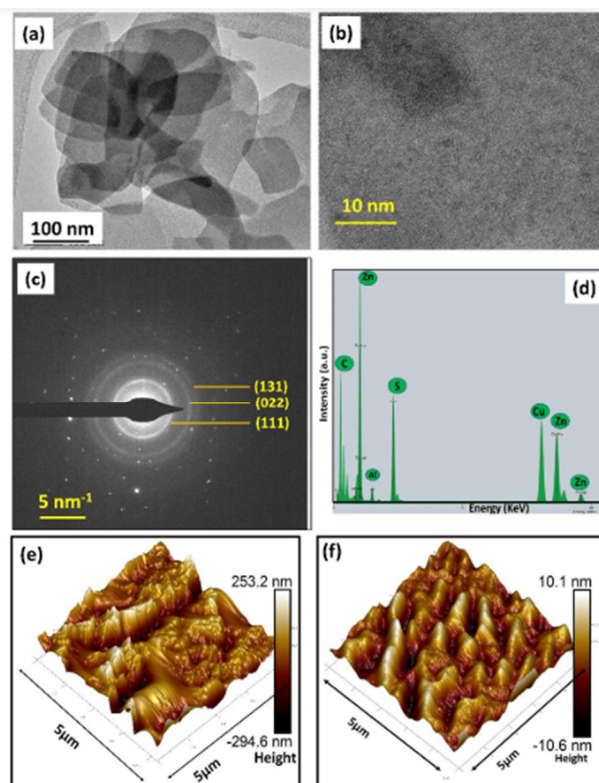


Figure 2 consists of the following images: (a) ZnS nanosheets as produced, (b) HRTEM picture of the same, (c) SAED pattern recorded on the same, (d) EDX spectrum obtained from a single ZnS nanosheet, (e) atomic force microscopy (AFM) of the same, and (f) AFM of PDMS.

1. First Experiment

The first step in mechanical energy harvesting was done to a $4 \times 4 \text{ cm}^2$ TENG with 1.5 cm between the tribolayers and force frequencies of around $3\text{-}4 \text{ Hz}$. In reaction to repetitive tapped with the hand, the TENG produces an open-circuit voltage, as shown in Figure 3(a). In the setup with the forward connection, a mean output voltage of around 7 Volts was noted. Figure 3(a) shows

the results of a polarity reversing test that included reversing the TENG connections and monitoring the output voltage with an oscilloscope. The findings showed that the voltage came straight from the TENG and not from any instrument noise, as it was the inverse of the forwarded signal. The TENG continued to show an average output voltage of around 8 V in the opposite connection as well. For both forwarded and reversed situations, Figure 3(b) shows the mean short-circuit current of our manufactured TENG device, which was around $6.21 \mu\text{A}$ and had a current density of about $0.28 \mu\text{A}/\text{cm}^2$. Compared to the values found in publications, the voltage output stated in this research is smaller (Table 1). Doped ZnS and heterostructure ZnS with ZnO are responsible for the greater output voltages shown in earlier studies. Nevertheless, neither doping nor heterostructures creation was used in this investigation. Both the forwarded and reversed conditions resulted in charges of around $0.050 \mu\text{C}$ and $0.015 \mu\text{C}$, respectively.

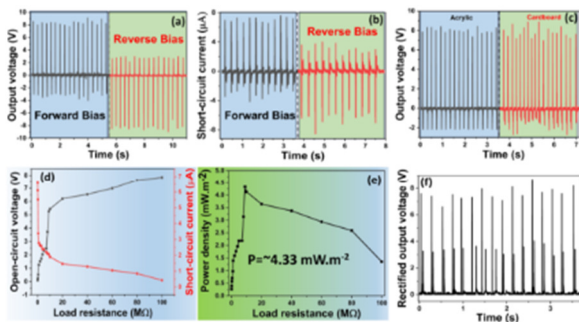


Figure 3 shows the following: (a) the forward-reverse output model of the TENG, (b) the forward-reverse shortcircuit current of the TENG, (c) the comparison of the output for 2 various bases, (d) the O/p voltage and current with various load resistance, (e) the output power with various load resistance, and (f) the rectified O/p voltage using a bridge rectifier.

2. Second Experiment

The second experiment involved the use of a cardboard base as the outer structure of the TENG in the place of the acrylic sheets. In terms of cost, cardboard turned out to be the better material for building the TENG device. The performance of the TENG based on the various base materials is depicted in Fig. 3(c) showing that the output of a $4 \times 4 \text{ cm}^2$ area and the 3-4 Hz applied force frequency is almost similar. As a result, the TENG developed on the cardboard substrate was selected for further investigations. The TENG's open-circuit voltage and short-circuit current were then measured at different load resistance levels ranging from $100 \text{ K}\Omega$ to $100 \text{ M}\Omega$ under uniform hand tapping to identify the peak output power. Figure 3(d) shows the voltage and current as a

function of the load resistance. By increasing the load resistance, the voltage increases and reaches a limiting value of approximately 7V . 85 V and the current begins from $6.588 \mu\text{A}$ with a $50 \text{ K}\Omega$ load resistance and then reduces to $0.43 \mu\text{A}$.

To investigate the roles of ZnS and PDMS in generating the TENG's output voltage, two additional TENGs were fabricated: TENG1, which includes only ZnS nanosheets with Al foil for the TENG structure, and TENG2 with only an Al substrate coated with PDMS. The TENG with both ZnS and PDMS was referred as TENG3 for convenience. The output voltages of all TENG devices in response to hand tapping and their circuit diagrams are shown in Fig. 4(a)–(e) for TENG1, TENG2, and TENG3. Open-circuit output voltages of approximately 472 mV , 3.60 V , and 8.02 V were recorded for TENG1, TENG2, and TENG3 correspondingly. The incorporation of ZnS nanosheets on the Al substrate (TENG3) increased the value by 2. A 25-fold increase in output voltage over a TENG device that incorporates only pure Al (TENG2). The increase in TENG output is explained by surface roughness, as previously mentioned in the literature. Tribolayer surface area, surface roughness, and electron affinity are the main determinants of the TENG's output performance. The output voltage of the TENG may be enhanced by increasing the surface roughness, which increases the surface area and the number of contact points. The results of this research corroborate those of earlier ones, which found that the output voltage of TENGs rises as surface roughness rises.

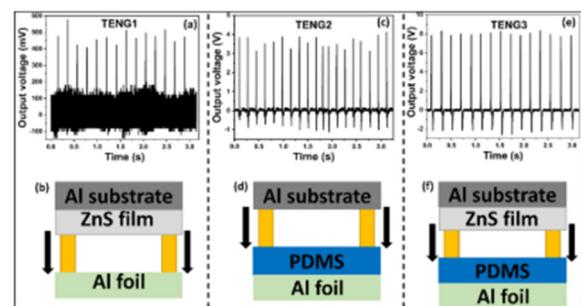


Figure 4: (a) O/p voltage of TENG1, (b) Layout of TENG1, (c) O/p voltage of TENG2, (d) Layout of TENG2, (e) O/p voltage of TENG3, (f) Layout of TENG3.

It is essential for the TENG to operate stably and maintain longevity to enable its use in real-life situations. The output voltage was monitored continually under the hand tapping force, which was applied

throughout the durability test for 1310 cycles, as shown in Figure 5(a). The average voltage of 44.34V for the 1310 cycles also proves the stability of the TENG developed in this work. Even more, the presented experiments have demonstrated the application of the vertical contact separation mode that has less impact on the physical destruction of the tribolayers. Therefore, both the ZnS nanosheets and the PDMS layers in the contact interface do not exhibit significant surface deformation during the frictional process which maintains the output voltage after 1000 cycles. Figure 5(b) shows an expansion of the stability graph focused on several cycles. The Figure 5 (c) depicts the oscillation of the average output voltage for every cycle.

When tested over shorter time durations like one month, two months and three months respectively, the TENG output voltage were virtually similar for all the tested conditions as illustrated in figure 5(d). The repeatability of these results was confirmed by the testing of six different nanogenerators that were produced under similar environment. Further, where the electrochemical durability of the ZnS nanostructure after 1310 cycles was investigated by scanning electron microscopy (SEM), no appreciable surface degradation observed, are depicted in Figures 5(e and f). The SEM results imply that the morphology of the ZnS nanosheets did not significantly change and that any slight transformation on the surface of the nanosheets would not significantly affect the output voltage of the nanogenerator.

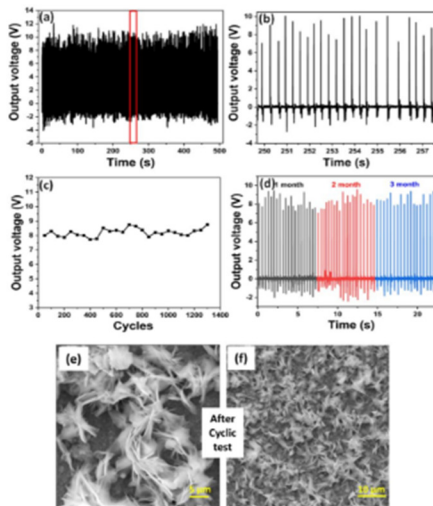


Figure 5 shows the following: (a) The stability of the TENG less than 1300 cycles, (b) An extended point of a few cycles, (c) the variance of the average O/p voltage as a function of every 50th cycle, (d) The stability of the TENG over various period intervals. Panels (e-f) show how it looks after the cyclic test at various magnifications

IV. RESULTS AND DISCUSSIONS

Figure 6(a) shows the initial results of recording the TENG reaction to various hand-tapping pressures. Figure 6(b) displays a picture of the TENG attached to an oscilloscope and positioned on a weighing scale. Under varying hand-tapping forces, the oscilloscope captured TENG's reaction in tandem with the weight values reported on the weighing scale. The output voltage variation is shown as a force function in Figure 6(c). Linear relation between force and TENG output voltage is clearly seen in Figure 6(c). According to the research, there is a consistent pattern in the TENG's reaction to various applied pressures [13]. Thus, when its output is adjusted to predetermined pressure values, the suggested TENG may be used as a force sensor. The curve's shape is rather non-linear. Therefore, an equation including a force as the independent variable and an output voltage as the dependent variable was developed by performing curve fitting in Origin software. An estimated ~6.52% inaccuracy was made for each accessible data point. Therefore, when a force value is provided, this formula may be used to immediately determine the appropriate O/P voltage of our TENG equipment.

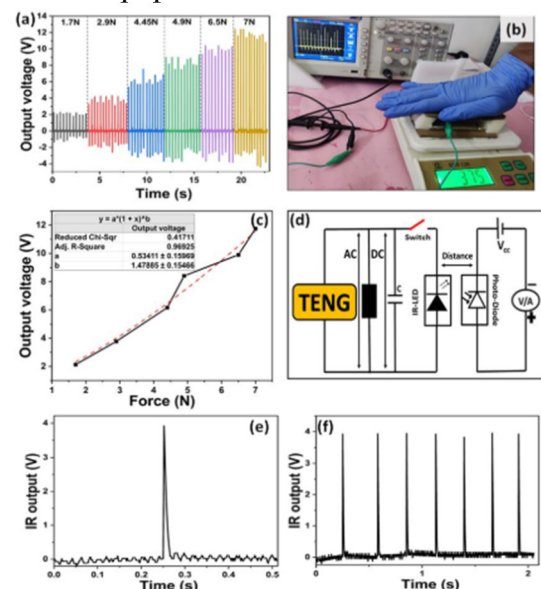


Figure 6: (a) The produced TENG's O/p response to various applied forces, (b) the original photograph of the testing, (c) the mean O/p voltage of the wireless pressure/force sensing circuit, (d) layout of the circuit connections, (e) the O/p voltage of infrared sensor, and (f) the repeatable O/p of the infrared sensor.

V. CONCLUSION

An optimized triboelectric nanogenerator (TENG) constructed from inexpensive inorganic substances is shown in this chapter. This chapter delves into the production of a TENG using ZnS nanosheet arrays, which is the first investigation into this method. A manually operated stimulation force of around 5.15 N was used to achieve the maximum output of about 8 V and 7.12 μ A. Additionally, digital circuits may employ the fabrication TENG as a self-sustaining clock pulse.

nanogenerator output performance by laser 3D-Surface pattern method for energy harvesting application." *Nano Energy* 78 (2020): 105205

REFERENCES

- [1] [1].Xia, Xin, Qing Liu, Yuyan Zhu, and Yunlong Zi. "Recent advances of triboelectric nanogenerator based applications in biomedical systems." *EcoMat* 2, no. 4 (2020): e12049.
- [2] [2] Shabbir, Irfan, Najaf Rubab, Tae Whan Kim, and Sang-Woo Kim. "Healthcare management applications based on triboelectric nanogenerators." *APL Materials* 9, no. 6 (2021).
- [3] [3] Li, Jiarong, Changsheng Wu, Ishara Dharmasena, Xiaoyue Ni, Zihan Wang, Haixu Shen, Shao-Lun Huang, and Wenbo Ding. "Triboelectric nanogenerators enabled internet of things: A survey." *Intelligent and Converged Networks* 1, no. 2 (2020): 115-141.
- [4] [4] Zhou, Yuankai, Maoliang Shen, Xin Cui, Yicheng Shao, Lijie Li, and Yan Zhang. "Triboelectric nanogenerator based self-powered sensor for artificial intelligence." *Nano Energy* 84 (2021): 105887.
- [5] [5] Yu, Ruomeng, Wenzhuo Wu, Yong Ding, and Zhong Lin Wang. "GaN nanobelt-based strain-gated piezotronic logic devices and computation." *ACS nano* 7, no. 7 (2013): 6403-6409.
- [6] [6] Wang, Zhong Lin, and Jinhui Song. "Piezoelectric nanogenerators based on zinc oxide nanowire arrays." *Science* 312, no. 5771 (2006): 242-246.
- [7] [7] Bai, Peng, Guang Zhu, Zong-Hong Lin, Qingshen Jing, Jun Chen, Gong Zhang, Jusheng Ma, and Zhong Lin Wang. "Integrated multilayered triboelectric nanogenerator for harvesting biomechanical energy from human motions." *ACS nano* 7, no. 4 (2013): 3713-3719.
- [8] [8] Lee, Minbaek, Chih - Yen Chen, Sihong Wang, Seung Nam Cha, Yong Jun Park, Jong Min Kim, Li - Jen Chou, and Zhong Lin Wang. "A hybrid piezoelectric structure for wearable nanogenerators." *Advanced materials* 24, no. 13 (2012): 1759-1764.
- [9] [9] Wang, Zhong Lin. "On Maxwell's displacement current for energy and sensors: the origin of nanogenerators." *Materials today* 20, no. 2 (2017): 74-82.
- [10] [10] Pan, Shuaihang, and Zhinan Zhang. "Fundamental theories and basic principles of triboelectric effect: A review." *Friction* 7 (2019): 2-17.
- [11] [11] Shao, Jiajia, Morten Willatzen, and Zhong Lin Wang. "Theoretical modeling of triboelectric nanogenerators (TENGs)." *Journal of Applied Physics* 128, no. 11 (2020).
- [12] [12] Yang, Bao, Wei Zeng, Ze - Hua Peng, Shi - Rui Liu, Ke Chen, and Xiao - Ming Tao. "A fully verified theoretical analysis of contact - mode triboelectric nanogenerators as a wearable power source." *Advanced Energy Materials* 6, no. 16 (2016): 1600505.
- [13] [13] Chun, Jinsung, Byeong Uk Ye, Jae Won Lee, Dukhyun Choi, Chong-Yun Kang, Sang-Woo Kim, Zhong Lin Wang, and Jeong Min Baik. "Boosted output performance of triboelectric nanogenerator via electric double layer effect." *Nature communications* 7, no. 1 (2016): 12985.
- [14] [14] Chung, C. K., and K. H. Ke. "High contact surface area enhanced Al/PDMS triboelectric nanogenerator using novel overlapped microneedle arrays and its application to lighting and self-powered devices." *Applied Surface Science* 508 (2020): 145310.
- [15] Muthu, Manikandan, Rajagopalan Pandey, Xiaozhi Wang, Arunkumar Chandrasekhar, I. A. Palani, and Vipul Singh. "Enhancement of triboelectric